Characterization of the apicoplast-localized enzyme *Tg*UroD in *Toxoplasma gondii* reveals a key role of the apicoplast in heme biosynthesis

Edwin T. Tjhin[‡], Jenni A. Hayward[‡], Geoffrey I. McFadden[§], and Giel G. van Dooren[‡1]

From the [‡]Research School of Biology, Australian National University, Canberra, ACT 2601, Australia, and the [§]School of BioSciences, University of Melbourne, Parkville, VIC 3010, Australia.

Running title: *The heme biosynthesis enzyme UroD in* Toxoplasma

[1]To whom correspondence may be addressed. Tel.: 61-2-6125-0665; E-mail: giel.vandooren@anu.edu.au.

Keywords: *Toxoplasma gondii*, Apicomplexa, heme biosynthesis, apicoplast, mitochondria, uroporphyrinogen III decarboxylase, cytochrome, cytochrome *c*/c_1 heme lyase.

ABSTRACT

Apicomplexan parasites such as *Toxoplasma gondii* possess an unusual heme biosynthesis pathway whose enzymes localize to the mitochondrion, cytosol or apicoplast, a non-photosynthetic plastid present in most apicomplexans. To characterize the involvement of the apicoplast in the *T. gondii* heme biosynthesis pathway, we investigated the role of the apicoplast-localized enzyme uroporphyrinogen III decarboxylase (*Tg*UroD). We found that *Tg*UroD knockdown impaired parasite proliferation, decreased free heme levels in the parasite, and decreased the abundance of heme-containing *c*-type cytochrome proteins in the parasite mitochondrion. We validated the effects of heme loss on mitochondrial cytochromes by knocking down cytochrome *c*/c_1 heme lyase 1 (*Tg*CCHL1), a mitochondrial enzyme that catalyzes the covalent attachment of heme to *c*-type cytochromes. *Tg*CCHL1 depletion reduced parasite proliferation and decreased the abundance of *c*-type cytochromes. We further sought to characterize the overall importance of *Tg*UroD and *Tg*CCHL1 for both mitochondrial and general parasite metabolism. *Tg*UroD depletion decreased cellular ATP levels, mitochondrial oxygen consumption, and extracellular acidification rates. By contrast, depletion of *Tg*CCHL1 neither diminished ATP levels in the parasite nor impaired extracellular acidification rate, but resulted in specific defects in mitochondrial oxygen consumption. Together, our results indicate that the apicoplast has a key role in heme biology in *T. gondii* and is important for both mitochondrial and general parasite metabolism. Our study highlights the importance of heme and its synthesis in these parasites.

Apicomplexans are a diverse phylum of intracellular parasites, containing species of medical, veterinary and agricultural importance. Of particular note are *Plasmodium* spp., the causative agents of malaria, and *Toxoplasma gondii*, the causative agent of toxoplasmosis. Most apicomplexan parasites possess a reduced plastid organelle, the apicoplast (1-3), that was derived from an endosymbiotic event whereby the heterotrophic ancestor of the apicomplexans engulfed a chloroplast-containing red alga (4,5). During the shift to parasitism, apicomplexans lost the need and ability for photosynthesis, resulting in a reduction in plastid functions (6). Apicoplasts are no longer photosynthetic but are predicted to play a variety of functionally important roles, including in heme biosynthesis (2,5,7,8).

Heme is a ubiquitous molecule that functions in a variety of essential life processes (7-9). Heme is a porphyrin molecule that consists of a cyclic tetrapyrrole structure with a central iron atom. The dual oxidation states of iron (which can exist as either Fe(II) or Fe(III)) allows heme to exist in either a reduced or an oxidized state (7,9), enabling

heme (and proteins containing heme as a prosthetic group) to participate in various electron transport and redox reactions. For example, heme is an important component of the mitochondrial electron transport chain (ETC^2) (8-10). Complex III (coenzyme Q:cytochrome *c* oxidoreductase) and Complex IV (cytochrome *c* oxidase) of the ETC contain heme molecules or heme-containing proteins (called cytochromes) that facilitate the transfer of electrons through these complexes, and the hemoprotein cytochrome *c* acts as an electron carrier between Complexes III and IV (8-10).

To obtain sufficient quantities of heme for their requirements, most eukaryotes possess a heme biosynthesis pathway (7). Although most of the heme biosynthesis enzymes are conserved amongst eukaryotes, the localization of these enzymes differs between different phyla (8). In animals, heme biosynthesis enzymes localize variously to the cytosol or mitochondrion, with final enzymes of the pathway occurring in the mitochondrion, the organelle that requires most heme in these organisms (8). By contrast, the heme biosynthesis pathway of plants, which shares numerous enzymes with the chlorophyll biosynthesis pathway, localizes predominantly to the plastid (8). The apicomplexan heme biosynthesis pathway is an unusual hybrid between the animal and plant pathways, with the eight enzymes in this pathway dispersed between the mitochondrion, cytosol and apicoplast (8,11). This unusual distribution likely evolved from reduction of the two heme biosynthesis pathways that existed in the ancestral apicomplexan host and its red algal symbiont early in apicomplexan evolution, leading to the hybrid pathway that exists today (12).

Like in animals, the first enzyme in the apicomplexan heme biosynthesis pathway localizes to the mitochondrion, synthesizing δ-aminolevulinic acid (ALA) from glycine and succinyl-CoA (13). ALA is then thought to be transported out of the mitochondrion and into the apicoplast (8). The next four enzymes are predicted to localize to the apicoplast, mirroring the heme synthesis pathway that occurs in plant plastids. Uroporphyrinogen III decarboxylase (UroD) is predicted to catalyze the final apicoplast-localized step of heme synthesis in apicomplexans, mediating the decarboxylation of uroporphyrinogen III to form coproporphyrinogen III (8). Coproporphyrinogen III is thought to be transported from the apicoplast into the cytosol, where it is oxidized. The final two enzymes, like in the animal pathway, localize back in the mitochondrion where heme is synthesized as the final product (14-16).

Numerous studies have examined the contribution of various enzymes in this "hybrid" heme biosynthesis pathway to the viability of *Plasmodium* parasites across the parasite life cycle. These studies have demonstrated that the pathway is dispensable in blood stages, where parasites likely scavenge heme from host erythrocytes, but important in insect and liver stages of the parasite life cycle (14,16-18). Although it is clear that the heme biosynthesis pathway is important for *Plasmodium* parasites to complete their life cycle, the role of synthesized heme is these parasites is not well understood. One study demonstrated that parasite-synthesized heme is incorporated into parasite proteins (16), and another predicts the presences of numerous hemoproteins in these parasites (8). The role of these putative hemoproteins in parasite biology, however, remain to be elucidated.

In contrast to the limited host cell range of *Plasmodium* parasites, *T. gondii* is capable of infecting virtually all nucleated cells in warm-blooded animals. Porphopbilinogen synthase, the second enzyme of the heme biosynthesis pathway, localizes to the apicoplast of *T. gondii*, and inhibitors of this enzyme impair parasite proliferation (19). Beyond this, the contribution of the parasite heme biosynthesis pathway to heme levels in *T. gondii*, and the importance of these enzymes for parasite proliferation and specific biological processes, have not been characterized.

In this study, we utilized genetic, biochemical, and physiological approaches to show that the apicoplast-localized heme biosynthesis enzyme *Tg*UroD is important for parasite proliferation and various biological processes within the parasite. Specifically, we demonstrate the importance of *Tg*UroD for the stability of heme-containing mitochondrial cytochromes, ETC function, and general parasite metabolism. Taken together, our data elucidate the importance of the apicoplast in a range of metabolic processes in these parasites.

RESULTS

_Tg_UroD is expressed in tachyzoites and localizes to the apicoplast

To determine if *Tg*UroD (www.toxodb.org accession number TGME49_289940) is expressed in the disease-causing tachyzoite stage of *T. gondii*, we integrated a 3 × hemagglutinin (HA) tag into the 3' region of the open reading frame in the native *Tg*UroD locus. Western blotting revealed the presence of two protein isoforms, one of ~70 kDa and a second of ~57 kDa (Fig. 1A). Immunofluorescence assays revealed that *Tg*UroD localized to a single, punctate structure in the parasite, overlapping with the apicoplast marker *Tg*Cpn60 (Fig. 1B). We conclude that *Tg*UroD is an apicoplast-localized enzyme, with the two molecular mass species likely the precursor and mature forms of the protein that are commonly observed in apicoplast-targeted proteins (20).

_Tg_UroD is important for tachyzoite proliferation

To facilitate a functional characterization of *Tg*UroD in *T. gondii*, we generated a regulatable knockdown strain (which we term r*Tg*UroD) wherein the native promoter of *Tg*UroD was replaced with an anhydrotetracycline (ATc)-regulatable promoter. Successful integration of the ATc-regulatable promoter was verified through PCR analysis (Fig. S1).

To determine whether *Tg*UroD expression could be down-regulated upon the addition of ATc, we integrated a c-Myc tag into the 3' end of the *Tg*UroD open reading frame, generating a strain we termed r*Tg*UroD-c-Myc. We grew parasites in the presence of ATc for 0 to 3 days and performed western blotting on protein extracts. This revealed that the high molecular mass precursor species of *Tg*UroD-c-Myc was undetectable after 1 day on ATc, and both molecular mass species were undetectable after two days (Fig. 2A).

To determine the importance of *Tg*UroD for parasite proliferation, we introduced a tandem dimeric Tomato red fluorescent protein into the r*Tg*UroD line, generating a Tomato/r*Tg*UroD cell line. We inoculated wells of a 96-well plate with Tomato/r*Tg*UroD or parental (Tomato/TATiΔ*ku80*) strain parasites, grew parasites in the absence or presence of ATc, and measured well fluorescence daily as a proxy for parasite proliferation, as previously described (21). Addition of ATc caused no difference in growth of the parental strain but severely impaired parasite proliferation in the Tomato/r*Tg*UroD strain (Fig. 2B-C). Complementation of the Tomato/r*Tg*UroD cell line with a constitutively expressed, HA-tagged copy of *Tg*UroD (a strain we termed c*Tg*UroD-HA/Tomato/r*Tg*UroD) largely restored parasite proliferation in the presence of ATc (Fig. 2D). We conclude that *Tg*UroD is important for tachyzoite proliferation.

Depletion of _Tg_UroD leads to reduced heme levels and reduced abundance of mitochondrial *c*-type cytochromes

Next, we asked whether *Tg*UroD was important for maintaining free heme levels in the parasite. To test this, we established a chemiluminescence assay based on the activity of the heme-requiring protein horseradish peroxidase (HRP; (22)). We grew r*Tg*UroD parasites in the absence or presence of ATc for 3 days, extracted whole cell lysates containing free heme, mixed these with apo-HRP, which is inactive in the absence of an exogenous source of heme, and measured chemiluminescence. Following calibration of HRP activity with known amounts of heme, this allowed us to estimate free heme levels in parasite. We found that parasites grown in the presence of ATc showed a significant, 6-fold reduction in the levels of free heme compared to parasites grown in the absence of ATc (Fig. 3A; $P = 0.032$, two-tailed unpaired Student's *t*-test, $n = 3$). This is consistent with the hypothesis that parasites lacking *Tg*UroD are unable to synthesize heme *de novo*.

To investigate the downstream effects of heme depletion in *Tg*UroD knockdown parasites, we examined the abundance of the heme-containing *c*-type cytochromes in the parasite. *C*-type cytochromes include cytochrome *c* (Cyt *c*) and cytochrome c_1 (Cyt c_1), proteins with central roles in electron transfer reactions in the ETC of the mitochondrion (10). Two homologues of Cyt *c* are encoded in the *T. gondii* genome, which we term Cyt *c*-A and Cyt *c*-B (10). We incorporated an HA-epitope tag into the 3' end of both the Cyt *c*-A and Cyt *c*-B open reading frames, and a 3 × c-Myc tag into the 3' end of the Cyt c_1 open reading frame, in the r*Tg*UroD-c-Myc or r*Tg*UroD parasite strains. We verified expression and mitochondrial localization of the tagged proteins by immunofluorescence assays (Fig. S2A-C).

We grew the resultant strains in ATc for 0-4 days and performed western blotting to measure changes in hemoprotein abundance. Cyt *c*-A abundance progressively decreased after 2 days on ATc, becoming virtually undetectable after 4 days (Fig. 3B). Cyt *c*-B protein was barely detectable after 3 days on ATc (Fig. 3C). c-Myc-tagged Cyt c_1 was more difficult to detect, but also appeared to decrease in abundance upon prolonged ATc exposure (Fig. 3D). These data indicate that the abundance of *c*-type cytochrome hemoproteins decreased upon *Tg*UroD knockdown.

Depletion of cytochrome *c*/c_1 heme lyase results in a decrease in cytochrome *c* abundance

The observation that mitochondrial hemoprotein levels decrease upon knockdown of *Tg*UroD led us to hypothesize that loss of heme synthesis leads to the inability of parasites to add heme prosthetic groups to these protein. In turn, the lack of a heme moiety may cause instability, and subsequent degradation, of these proteins. Heme is covalently attached to *c*-type cytochromes in a reaction catalyzed by cytochrome *c*/c_1 heme lyases (CCHLs; (8,23)). The *T. gondii* genome encodes two candidate CCHL enzymes, which we termed *Tg*CCHL1 (TGME49_293390) and *Tg*CCHL2 (TGME49_314042). With a view to understanding the importance of heme prosthetic groups for the stability of *c*-type cytochromes, we set out to characterize the roles of these CCHL proteins in the maturation of *c*-type cytochromes in *T. gondii*.

We first investigated the role of *Tg*CCHL1 protein in *T. gondii* biology. We generated a regulatable knockdown strain of *Tg*CCHL1 wherein the native promoter was replaced with an ATc-regulatable promoter, simultaneously integrating a 3×HA-tag into the 5' end of the *Tg*CCHL1 open reading frame (Fig. S3A). Successful integration of the ATc-regulatable promoter was verified through PCR analysis (Fig. S3B-C). We termed the resultant parasite strain rHA-*Tg*CCHL1.

We performed an immunofluorescence assay and found that HA-*Tg*CCHL1 localized to the parasite mitochondrion (Fig. 4A). We then performed western blotting on proteins extracted from rHA-*Tg*CCHL1 parasites grown in the presence of ATc for 0-3 days and found that HA-*Tg*CCHL1 was undetectable after 2 days on ATc (Fig. 4B).

To determine the importance of *Tg*CCHL1 for parasite proliferation we performed plaque assays. We grew rHA-*Tg*CCHL1 parasites in the absence or presence of ATc for 8 days and observed the formation of zones of clearance ('plaques') in the host cell monolayer, the sizes of which correlate with parasite proliferation. Plaque formation in rHA-*Tg*CCHL1 parasites grown in the presence of ATc was severely impaired, whereas parental TATiΔ*ku80* strain parasites grew normally (Fig. 4C). This suggests that *Tg*CCHL1 is important for parasite proliferation.

Next, we investigated the importance of *Tg*CCHL1 for the abundance of *c*-type cytochromes. We incorporated a HA tag into the into the 3' region of the Cyt *c*-B open reading frame, or a c-Myc tag into the 3' region of the Cyt c_1 locus, in rHA-*Tg*CCHL1 strain parasites. We then monitored the abundance of *c*-type cytochromes upon HA-*Tg*CCHL1 knockdown. We grew parasites for 0 to 4 days in ATc and measured protein abundance by western blotting, utilizing an anti-Cyt *c*-A antibody (24) to detect Cyt *c*-A. Cyt *c*-A was virtually undetectable after 2 days in ATc (Fig. 4D). Cyt *c*-B-HA abundance decreased considerably after 2 days and was undetectable after 3 days (Fig. 4E). Cyt c_1-c-Myc was again difficult to detect, but its abundance appeared to decrease after 4 days (Fig. 4F). We conclude that knockdown of *Tg*CCHL1 results in a depletion of mitochondrial *c*-type cytochromes, which mirrors the effect we observe upon *Tg*UroD knockdown. This is consistent with the hypothesis that integration of the heme prosthetic group is important for stabilizing *c*-type cytochromes, and that loss of heme synthesis upon *Tg*UroD knockdown leads to defects in the abundance of these proteins.

We also examined the importance of *Tg*CCHL2 for *T. gondii* proliferation. We replaced the native promoter of *Tg*CCHL2 with an ATc-regulatable promoter to generate a strain we termed r*Tg*CCHL2 (Fig. S4A), verifying successful integration by PCR analysis (Fig. S4B-E). We measured proliferation of r*Tg*CCHL2 parasites in the presence or absence of ATc by plaque assay. We observed no obvious defects in proliferation in the r*Tg*CCHL2 strain cultured in the presence of ATc compared to the parental control (Fig. S4F). As we did not incorporate an epitope tag into *Tg*CCHL2 locus, we could not verify successful knockdown of the *Tg*CCHL2 protein upon the

addition of ATc. However, our observations are in line with a genome-wide phenotypic screen of *T. gondii* parasites, which predicted that *Tg*CCHL2 is dispensable for tachyzoite proliferation (25). Given the lack of a growth phenotype in our mutant, we did not pursue the role of *Tg*CCHL2 in parasites any further.

Investigating the importance of heme biosynthesis in parasite metabolism

We next sought to establish the role of heme biosynthesis in parasite metabolism. Given the importance of *c*-type cytochromes in the mitochondrial ETC, and the role of the ETC in mitochondrial ATP synthesis (10,26), we reasoned that knockdown of *Tg*UroD would lead to defects in ATP levels in the parasite. We measured ATP levels in r*Tg*UroD parasites grown in the presence or absence of ATc and found significantly lower amounts of cellular ATP upon *Tg*UroD knockdown (Fig. 5A; $P = 0.008$, two-tailed unpaired Student's *t*-test, $n = 3$). To determine whether this decrease in ATP levels resulted from the effects of *Tg*UroD knockdown on mitochondrial cytochromes, we measured ATP levels in rHA-*Tg*CCHL1 parasites grown in the absence or presence of ATc. Surprisingly, we found no significant change in ATP levels upon HA-*Tg*CCHL1 knockdown (Fig. 5B; $P = 0.738$, two-tailed unpaired Student's *t*-test, $n = 3$). This indicates that parasites are able to maintain cellular ATP levels despite the decrease in mitochondrial hemoprotein abundance that occurs upon *Tg*CCHL1 knockdown, and suggests that the effects of *Tg*UroD knockdown on parasite ATP levels are independent of their effect on *c*-type cytochrome abundance.

To further investigate mitochondrial function upon knockdown of *Tg*UroD, we measured mitochondrial membrane potential ($\Delta\Psi_m$) using the dye JC-1, as described previously (27). The mitochondrial ETC mediates ATP generation by establishing of a proton gradient across the inner mitochondrial membrane (10), and we reasoned that the defects in *c*-type cytochrome abundance upon *Tg*UroD knockdown would impair the ETC, which would lead to a depletion of $\Delta\Psi_m$. As predicted, knockdown of *Tg*UroD resulted in a dissipation of $\Delta\Psi_m$ (Fig. S5). To determine whether this change in $\Delta\Psi_m$ resulted selectively from impairment of mitochondrial cytochromes, we measured $\Delta\Psi_m$ upon *Tg*CCHL1 knockdown. Surprisingly, we found that knockdown of *Tg*CCHL1 did not impair $\Delta\Psi_m$ (Fig. S5). This indicates that mitochondrial membrane potential can be maintained in the absence of detectable amounts of *c*-type cytochromes, and that the defects in $\Delta\Psi_m$ that we observe upon *Tg*UroD knockdown are probably independent of the downregulation of mitochondrial cytochromes that result from impairing parasite heme synthesis.

Loss of $\Delta\Psi_m$ can be indicative of a general loss of cell viability (28), and we therefore sought an alternative measure of ETC function upon *Tg*UroD knockdown. We grew *Tg*UroD parasites in the absence of ATc, or in the presence of ATc for 3 or 4 days and measured mitochondrial oxygen consumption rate (mOCR) using a Seahorse XFe96 flux analyzer, as described previously (29). We observed a significant decrease in mOCR upon *Tg*UroD knockdown (Fig. 5C; $P < 0.001$, linear mixed model ANOVA, $n = 3$). This indicates that depletion of *Tg*UroD, and concomitant loss of heme synthesis, leads to defects in ETC function. We observed a similar, significant decrease in mOCR upon *Tg*CCHL1 knockdown (Fig. 5D; $P < 0.001$, linear mixed model ANOVA, $n = 3$), indicating that depletion of *c*-type cytochromes also results in defects in ETC function.

The Seahorse XFe96 flux analyzer also measures the rate at which parasites acidify their extracellular environment (29). In mammalian cells, extracellular acidification rate (ECAR) corresponds primarily to glycolytic activity (30). Whether ECAR in *T. gondii* is a specific measure for glycolysis, or whether other metabolic processes in the parasite also contribute to ECAR, has not been experimentally demonstrated. Nevertheless, we have used ECAR as a general measure for parasite metabolic activity (29). We found that knockdown of *Tg*UroD resulted in a significant ~80% decrease in ECAR (Fig. 5E; Fig. S6A; $P < 0.001$, linear mixed model ANOVA, $n = 3$). By contrast, knockdown of *Tg*CCHL1 resulted in a significant ~30% *increase* in ECAR (Fig. 5F; Fig. S6B; $P = 0.045$ and $P = 0.001$ after 3 days and 4 days on ATc, respectively, linear mixed model ANOVA, $n = 3$). These data are consistent with knockdown of *Tg*UroD resulting in a general impairment of parasite metabolism, whereas *Tg*CCHL1 knockdown appears to result in a selective defect in the mitochondrial ETC and a concomitant increase in other aspects of parasite metabolism.

DISCUSSION

In this study, we have demonstrated that *Tg*UroD, an apicoplast-localized enzyme, is important for survival and proliferation of the disease-causing tachyzoite stage of the *T. gondii* life-cycle. Knockdown of *Tg*UroD led to a decrease in free heme in the parasites (Fig. 3A), implying a key role for the apicoplast in parasite heme biosynthesis. Our data are consistent with a recent study by Bergmann and colleagues, who demonstrated that loss of mitochondrial and cytosolic heme biosynthesis enzymes led to defects in *T. gondii* proliferation, virulence and heme levels (31).

Knockdown of *Tg*UroD resulted in a decrease in the abundance of heme-containing *c*-type cytochrome proteins in the parasite mitochondrion (Fig. 3B-D). We postulate that the decrease in free heme levels upon *Tg*UroD knockdown diminishes heme incorporation into *c*-type cytochromes, resulting in instability and subsequent degradation of these proteins. In support of this, we found that knockdown *Tg*CCHL1, an enzyme that catalyzes the covalent attachment of heme to *c*-type cytochromes (23), also resulted in a depletion in the abundance of *c*-type cytochromes (Fig. 4D-F). Our data also demonstrate that *Tg*UroD knockdown results in impairment of mitochondrial O_2 consumption in the parasite, a phenotype mirrored upon *Tg*CCHL1 knockdown (Fig. 5C-D). These data indicate a key role of heme in the ETC of the mitochondrion, both as part of *c*-type cytochromes, and likely also the *b*- and *a*-type cytochromes that occur in the coenzyme Q:cytochrome *c* oxidoreductase and cytochrome *c* oxidase complexes of the ETC (8,10). Our study, therefore, links apicoplast metabolism to a central function of the mitochondrion. Other products of apicoplast metabolism are also thought to be utilized in the mitochondrion, including isoprenoids (precursors of coenzyme Q) and fatty acids (precursors of lipids that are synthesized by the mitochondrion) (32). Together, these observations suggest that the apicoplast organelle plays a key "support" role for mitochondrial processes (32).

Our data demonstrate that knockdown of *Tg*UroD leads to a depletion in parasite ATP levels (Fig. 3A), an impairment in the ability of parasites to acidify their extracellular environment (Fig. 5E), and a loss of mitochondrial $\Delta\Psi_m$ (Fig. S5). These processes all require active parasite metabolism, pointing to a role for *Tg*UroD in maintaining metabolic processes in the parasite. The ECAR defects we observe upon *Tg*UroD knockdown resemble similar defects we have observed previously upon treating parasites with cycloheximide (29), a translation inhibitor that rapidly depletes protein synthesis leading to generalized cell death (33). Loss of mitochondrial $\Delta\Psi_m$ is also frequently interpreted as an indicator of cell death (28). In concert, these data suggest that knockdown of *Tg*UroD may lead to a general cell death response in the parasite. This response is probably independent of the impact of heme synthesis on the mitochondrial ETC and oxidative phosphorylation, since we did not observe defects in parasite ATP levels, ECAR or $\Delta\Psi_m$ upon *Tg*CCHL1 knockdown (Fig. 4B, Fig. 4F, Fig. S5), and have previously reported that knockdown of key proteins in the parasite cytochrome *c* oxidase and ATP synthase complexes do not impair ECAR (26,29).

One possibility is that heme is required for metabolic processes beyond the mitochondrial ETC. In addition to mitochondrial cytochrome proteins, the *T. gondii* genome encodes seven cytochrome b_5-containing proteins and a homologue of cytochrome P450 (8). The functions of these proteins are currently still unstudied, but one of the cytochrome b_5 proteins (TGME49_276110) is predicted to be important for parasite growth (25). Loss of heme synthesis is likely to impair the function of this and other non-mitochondrial ETC cytochromes, which may explain the resultant effects of *Tg*UroD knockdown on parasite metabolism and survival.

An alternative explanation for the postulated cell death phenotype is that knockdown of *Tg*UroD leads to a build-up of toxic porphyrin intermediates in the cell, similar to the effects observed in human porphyrias. Human porphyrias result from partial deficiencies in heme synthesis enzymes (34). A decrease in UroD activity in hepatic cells in humans is the cause for the most common porphyria in humans, termed porphyria cutanea tarda (35,36). Porphyria cutanea tarda results from the accumulation of uroporphyrinogen III (the substrate of UroD) and other by-products of heme synthesis, leading to oxidative stress and cell

death. This manifests as skin photosensitivity and the formation of skin lesions or blisters in affected patients. In a similar vein, the build-up of heme precursors in *Plasmodium*-infected erythrocytes results in parasite photosensitivity and a concomitant inhibition of parasite proliferation (37). It is conceivable then that a build-up of uroporphyrinogen III or other heme precursors upon *Tg*UroD knockdown may be toxic to parasite cells, leading to the cell death phenotypes we observed in our study.

Determining whether the cell death effect we observe upon *Tg*UroD knockdown results from a loss of heme synthesis and/or from the accumulation of toxic porphyrins will require further study. It will be of particular interest to examine whether similar cell death phenotypes are observed in heme biosynthesis pathway mutants that do not lead to the accumulation of potentially toxic porphyrins (e.g. mutants in δ-aminolevulinic acid synthase, the first enzyme of the pathway; (31)).

In addition to our examination of the heme biosynthesis pathway, our study examines the maturation and role of *c*-type cytochromes in the mitochondrial ETC of *T. gondii*. We demonstrate that knockdown of *Tg*CCHL1 leads to depletion of both cytochrome *c* isoforms in the parasite, as well as cytochrome c_1, a component of the coenzyme Q:cytochrome *c* oxidoreductase complex (Fig. 4D-F). In turn, this leads to a selective defect in mitochondrial O_2 consumption (Figs. 5D, 5F), as we have seen previously when inhibiting other components of the ETC (29). Notably, loss of *c*-type cytochromes upon *Tg*CCHL1 knockdown did not result in decreased ATP levels in the parasite (Fig. 5B) or in mitochondrial $\Delta\Psi_m$ (Fig. S5). This suggests that parasites can maintain $\Delta\Psi_m$ and generate ATP in the absence of a functional ETC. It is possible that parasites are able to upregulate ATP generation through glycolysis to compensate for defects in oxidative phosphorylation. Consistent with this, we observed a significant increase in ECAR upon *Tg*CCHL1 knockdown (Fig. 5F; Fig. S6B). ECAR is, in part, probably dependent on the extrusion of lactate from the parasite. Lactate is an end-product of anaerobic glycolysis, and the increase in ECAR we observe suggests that parasites respond to impairment of oxidative phosphorylation by increasing anaerobic glycolysis. This hypothesis is consistent with other studies that highlight considerable metabolic flexibility in central carbon metabolism in *T. gondii* parasites (38-43). These studies have revealed that parasites are able to utilize numerous carbon sources for energy generation (including glucose, glutamine, and storage products such as amylopectin and γ-aminobutyric acid), and are able to metabolize these substrates differently (e.g. anaerobic glycolysis vs aerobic glycolysis vs glutaminolysis) in different life stages, or when parasites lack enzymes involved particular aspects of central carbon metabolism. Examining the effects of *Tg*CCHL1 knockdown (and the concomitant loss of cytochrome maturation) on central carbon metabolism in the parasite may reveal how these parasites compensate for the predicted loss of mitochondrial ATP production.

Some eukaryotes, such as yeast, contain separate heme lyase enzymes for catalyzing heme attachment in cytochrome *c* and cytochrome c_1. (44). We observe a depletion of both cytochrome *c* isoforms and cytochrome c_1 upon *Tg*CCHL1 knockdown (Fig. 4D-F), consistent with *Tg*CCHL1 being capable of catalyzing the insertion of heme into all three *c*-type cytochromes in the parasite. We observe a more rapid depletion of the two cytochrome *c* isoforms than of cytochrome c_1 upon *Tg*CCHL1 knockdown (Fig. 4D-F). It is conceivable that the second parasite heme lyase, *Tg*CCHL2 (which is annotated as a cytochrome c_1 heme lyase on ToxoDB), may also be capable of inserting heme into cytochrome c_1, although it appears that *Tg*CCHL2 is not crucial for growth of *T. gondii* (Fig. S4; (25)), suggesting that its role is, at most, redundant with that of *Tg*CCHL1. Studies in yeast have demonstrated that CCHL enzymes, and the heme incorporation that they catalyze, is critical for the transport of cytochrome *c* into the mitochondrial inner membrane space (23,45). The more rapid depletion of the two cytochrome *c* isoforms than of cytochrome c_1 that we observe (Fig. 4D-F) may, therefore, result from degradation of cytochrome *c* associated with its inability to import into the mitochondrion of the parasite.

Overall, our study indicates that the apicoplast of *T. gondii* has an important role in *de novo* heme synthesis in the parasite, contributing to the mitochondrial ETC as well as to other metabolic processes in the parasite. Recent studies have highlighted the potential of heme biosynthesis as a drug target (31) and revealed the role of parasite

heme synthesis in modulating the susceptibility of apicomplexan parasites to existing drugs such as artemisinin (46). Our study, therefore, contributes to a growing body of literature that highlights the importance of understanding heme and its synthesis in these parasites.

EXPERIMENTAL PROCEDURES

Host cell and parasite culture and growth assays

T. gondii was cultured in human foreskin fibroblasts (HFF), as previously described (47). HFF cells were cultured in Dulbecco's modified Eagle's medium (DMEM) supplemented with 10% (v/v) bovine calf serum, 50 U/ml penicillin, 50 µg/ml streptomycin, 10 µg/ml gentamicin, 0.25 µg/ml amphotericin B and 0.2 mM L-glutamine. HFF cells were grown in tissue culture flasks in a humidified 5% CO_2 incubator set to 37°C. Parasites were grown in confluent HFF monolayers, and were incubated in supplemented DMEM containing 1% (v/v) foetal calf serum, 50 U/ml penicillin, 50 µg/ml streptomycin, 10 µg/ml gentamicin, 0.25 µg/ml amphotericin B and 0.2 mM L-glutamine (Ed1). Where applicable, ATc was added to culture medium at a final concentration of 0.5 µg/ml. Parasites in paired ATc experiments grown without ATc had ethanol added as a vehicle control. Fluorescence growth assays were performed as previously described (48,49). Parasites were cultured in phenol red-free Roswell Park Memorial Institute 1640 medium supplemented with 1% (v/v) foetal calf serum, 50 U/ml penicillin, 50 µg/ml streptomycin, 10 µg/ml gentamicin, 0.25 µg/ml amphotericin B and 0.2 mM L-glutamine (Ed1), and fluorescence was read daily using a FLUOstar OPTIMA microplate reader (BMG Labtech). Plaque assays were performed as previously described (47), with 500 parasites added per flask, and flasks incubated for 8-10 days before crystal violet staining.

Genetic modification of T. gondii

TATiΔ*ku80* strain parasites (50) were used as the parental cell line for generating the genetically modified parasites described in this study. To generate fluorescent parasites used in the fluorescence growth assays, we introduced tandem dimeric Tomato red fluorescent protein into the relevant cell lines, as previously described (49). All genetically modified parasite strains were cloned by limiting dilution or flow cytometry before being characterized.

To incorporate a 3' HA tag into the *Tg*UroD locus, we PCR amplified the 3' region of the *Tg*UroD gene with primers 1 and 2 (all primers listed in Table S1), and cloned the resulted product into the pLIC-3xHA/DHFR vector by ligation independent cloning, as described previously (51). The resulting vector was linearized with *Nsi*I before transfection into parasites and selection on pyrimethamine, as described previously (47).

To generate an ATc-regulatable *Tg*UroD parasite strain, we amplified the region including and immediately downstream of the *Tg*UroD start codon with primers 3 and 4. We digested this with *Bgl*II and *Not*I and ligated into the equivalent sites of the vector pPR2-HA_3 (52). We termed the resulting vector pPR2(TgUroD 3'flank). We next amplified a region upstream of the *Tg*UroD start codon with primers 5 and 6. We digested the resulting product with *Pac*I and *Nsi*I, and ligated into the equivalent sites of the pPR2(TgUroD 3'flank) vector. We linearized the resulting vector with *Not*I, transfected into parasites, and selected on pyrimethamine. Clonal parasites were screened for the presence of the native *Tg*UroD locus with primers 7 and 8, and for presence of the modified locus with primers 8 and 9. A 3' c-Myc tag was integrated into the ATc-regulatable *Tg*UroD locus by amplifying the 3' region of the *Tg*UroD gene using primers 10 and 11. The resulting product was digested with *Bgl*II and *Avr*II and ligated into the equivalent sites of the $pgCM_3$ vector (52). The resulting vector was linearized with *Pst*I, transfected into r*Tg*UroD strain parasites, and selected on chloramphenicol, as described (47).

To complement the r*Tg*UroD line with a constitutively expressed copy of *TgUroD*, we amplified the entire *Tg*UroD open reading frame using primers 11 and 12 and cDNA as template. We digested the resultant product with *Bgl*II and *Avr*II, and ligated this into the *Bgl*II and *Avr*II sites of the vector $pUgCTH_3$ (49). We linearized the resultant vector with *Mfe*I, transfected it into the r*Tg*UroD strain, and selected on chloramphenicol.

To incorporate a 3' HA tag in the *Tg*Cyt *c*-A locus, we amplified the 3' region of the *Tg*Cyt *c*-A open reading frame using the primers 13 and 14. We digested the resultant product with *Bgl*II and *Avr*II, and ligated this into the *Bgl*II and *Avr*II sites of the vector pgCH (49). The resultant vector was

linearized with *Mfe*I, transfected into the relevant parasite strains, and selected on chloramphenicol.

To incorporate a 3' HA tag in the *Tg*Cyt *c*-B locus, we amplified the 3' region of the *Tg*Cyt *c*-B open reading frame using the primers 15 and 16. We digested the resultant product with *Bgl*II and *Avr*II, and ligated this into the *Bgl*II and *Avr*II sites of the vector pgCH. The resultant vector was linearized with *Afe*I, transfected into the relevant parasite strains, and selected on chloramphenicol.

To incorporate a 3' c-Myc tag in the *Tg*Cyt-c_1 locus, we amplified the 3' region of the *Tg*Cyt-c_1 open reading frame using the primers 17 and 18. We digested the resultant product with *Bgl*II and *Avr*II, and ligated this into the *Bgl*II and *Avr*II sites of the vector pgCM$_3$. The resultant vector was linearized with *Pst*I, transfected into the relevant parasite strains, and selected on chloramphenicol.

To generate the *Tg*CCHL1 knockdown strain, we amplified the region including and immediately downstream of the *Tg*CCHL1 start codon with primers 19 and 20. The resultant PCR product was digested with *Xma*I and *Not*I and ligated into the equivalent sites of the pPR2-HA$_3$ vector, generating a vector we termed pPR2-HA$_3$(TgCCHL1 3' flank). We next amplified the region upstream of the *Tg*CCHL1 start codon with primers 21 and 22. We digested the resultant product with *Psp*OMI and *Nde*I, and ligated this into the equivalent sites of the pPR2-HA$_3$(TgCCHL1 3' flank) vector. We linearized the resulting vector with *Not*I, transfected into parasites, and selected on pyrimethamine. Clonal parasites were screened for the presence of the native *Tg*CCHL1 locus using primers 23 and 24, and presence of the modified locus using primers 9 and 24.

To generate the *Tg*CCHL2 knockdown cell line, we first amplified the 3' flank region of the *Tg*CCHL2 locus with primers 25 and 26. We digested the resultant product with *Avr*II and *Not*I, and ligated this into the equivalent sites of the vector pPR2-HA$_3$, generating a vector we termed pPR2(TgCCHL2 3'flank). We then amplified the 5' flank region of the *Tg*CCHL2 locus with primers 27 and 28. We digested the resultant product with *Apa*I and *Nde*I, and ligated this into the equivalent sites of the pPR2(TgCCHL2 3'flank) vector. The resultant vector was linearized with *Not*I, transfected into parasites, and selected on pyrimethamine. To verify successful integration of the construct, we used primer combinations 29/30 and 31/32 to test for the presence of the native *Tg*CCHL2 locus, and primer combinations 9/30 and 31/33 to test for the presence of the modified locus.

Immunofluorescence assays, SDS-PAGE and Western blotting

Immunofluorescence assays and SDS-PAGE/Western blotting were performed as described previously (21). The primary antibodies used were rat anti-HA (1:100 to 1:250; Roche clone 3F10), mouse anti-c-Myc (1:100 to 1:500; Santa Cruz Biotechnology clone 9E10), mouse anti-GRA8 (1:50,000 to 1:200,000; a kind gift from Gary Ward, U. Vermont; (53)), anti-Tom40 (1:2,000-3,000; (24)), anti-Cpn60 (1:2,000; (54)) and anti-Cyt *c*-A (1:250-1:500; (29)). Secondary antibodies used were HRP-conjugated goat anti-rat IgG (1:5,000; Santa Cruz Biotechnology cat #: sc-2006), HRP-conjugated goat anti-mouse IgG (1:5,000-10,000; Santa Cruz Biotechnology cat #: sc-2005), HRP-conjugated goat anti-rabbit IgG (1:5,000; Santa Cruz Biotechnology cat #: sc-2004), AlexaFluor 488-conjugated goat highly cross-adsorbed anti-rat IgG (1:250, Thermo Scientific cat #: A11006), AlexaFluor 488-conjugated goat highly cross-adsorbed anti-mouse IgG (1:200-250, Thermo Scientific cat #: A11029), AlexaFluor 546-conjugated goat highly cross-adsorbed anti-mouse IgG (1:250, Thermo Scientific cat #: A11030), AlexaFluor 546-conjugated goat anti-rabbit IgG (1:250, Thermo Scientific cat #: A11035), AlexaFluor 647-conjugated goat anti-rabbit IgG (1:250, Thermo Scientific cat #: A21244) and CF647-conjugated goat anti-rabbit (1:500, Sigma cat #: SAB4600177). Immunofluorescence images were acquired on a DeltaVision Elite system (GE Healthcare) using an inverted Olympus IX71 microscope with a 100 × UPlanSApo oil immersion lens (Olympus) paired with a Photometrics CoolSNAP HQ^2 camera, or on Leica TCS SP2 inverted laser scanning confocal microscope. Images taken on the DeltaVision setup were deconvolved using SoftWoRx Suite 2.0 software. Images were adjusted linearly for contrast and brightness. Western blots were exposed onto X-ray films and scanned.

Free heme measurements

Parasites were harvested from 175 cm^2 tissue culture flasks, passed through a 3 μm filter to remove host cell debris, then centrifuged at 1,500 × *g* for 10 min to pellet them. Free heme was extracted from parasite pellets by the addition of acidified acetone (100 % v/v acetone with 0.05 % v/v concentrated HCl). This was followed by 10 s of vigorous vortexing, 10 min of incubation on ice, and 10 min of incubation at ambient temperature. Cell debris was pelleted by centrifugation at 20,000 × *g* for 10 min at 4°C. Free heme in the supernatant was transferred to a separate tube, and the extraction was repeated with an acidified acetone/water solution mix (acidified acetone solution with 20 % v/v distilled water) Supernatants were pooled and were subsequently concentrated until dry using a Savant SpeedVac SC100 (Thermo Scientific) with no heat and protected from light.

A horseradish peroxidase (HRP)-based heme detection assay was adapted from (22). Apo-HRP was derived from HRP enzyme (Sigma) with Teale's butanone extraction method (55,56). Briefly, an equivolume of ice-cold 2-butanone was added to HRP (25 μM, pH 2.5 with HCl), mixed thoroughly and incubated at 4°C until clear layers formed. The top and middle layer were aspirated, leaving the bottom aqueous layer containing apo-HRP. An Illustra NAP-5 size exclusion column packed with Sephadex G-25 DNA Grade resin (GE-Healthcare Life Sciences) was used to filter and remove excess 2-butanone from the aqueous layer. The initial flow-through of the column was collected and the concentration of apo-HRP was calculated with a millimolar extinction coefficient of 20 at 278 nm.

Heme reconstitution reactions were set up with 10 nM of apo-HRP enzyme, 100 mM Tris-HCl pH 8.4 and 10 mM KOH. Heme solutions (known standards or cell extracts) were added at 10 % of the total reaction volume and incubated in white, non-treated, low auto-luminescence flat bottom 96 well plate (Nunc, Thermo Scientific) for 30 min at room temperature. An equivolume of reaction solution containing 10 mM luminol, 100 mM Tris-HCl pH 8.4 and 200 μM of H_2O_2 was added to start the reaction and luminescence was read immediately using a FLUOstar OPTIMA microplate reader (BMG Labtech). Heme concentration in the cell samples were calculated from a standard curve generated from known heme concentrations.

ATP measurements

Parasites were harvested from 175 cm^2 tissue culture flasks, passed through a 3 μm filter to remove host cell debris, then centrifuged at 1500 × *g* for 10 min to pellet them. Parasites were washed in Hanks' Balanced Salt Solution (Sigma), then resuspended in Buffer A with Glucose (116 mM NaCl, 5.4 mM KCl, 0.8 mM $MgSO_4$, 5.5 mM D-glucose, 5 mM HEPES, pH 7.2) to a concentration of 1×10^8 parasites/ml. Parasites were incubated in a 5% CO_2 incubator for 1 hour at 37°C, pelleted by centrifugation, and resuspended in a 1:1 mixture of Buffer A with Glucose and 0.5 M $HClO_4$. Parasite suspensions were incubated on ice for 30 minutes, then pelleted by centrifugation at 20,000 × *g* for 5 min at 4°C. The reaction was neutralized with 33.3% (v/v) neutralizing solution (0.72 M KOH, 0.16 M $KHCO_3$) and stored at -20°C or used immediately.

The Invitrogen ATP Determination Kit (Thermo Scientific cat. # A22066) was used to calculate ATP levels according to the manufacturer's instructions. Parasite extracts or ATP standards were added at 10% of the total volume of each reaction, and luminescence was read immediately after commencing the reaction on a FLUOstar OPTIMA microplate reader (BMG Labtech). ATP concentrations in the samples were calculated from a standard curve generated from known ATP concentrations.

Mitochondrial membrane potential ($\Delta\Psi_m$) measurements

Mitochondrial membrane potential was measured using the $\Delta\Psi_m$-sensitive dye 5,5',6,6'-Tetrachloro-1,1',3,3'-tetraethylbenzimidazolyl-carbocyanine iodide (JC-1), as described previously (27). Briefly, parasites were harvested, washed once in phenol red-free Ed1, and resuspended to 2.5×10^7 parasites/ml in Ed1. The protonophore carbonyl cyanide 3-chlorophenylhydrazone (CCCP) was added to the appropriate control tubes and incubated for 30 min. JC-1 was added to a final concentration of 1.5μM and parasites were incubated for 15 min before being analyzed by flow cytometry using a BD FACSCalibur (Becton Dickinson) flow cytometer.

Seahorse XFe96 flux analysis

Seahorse XFe96 flux analysis experiments were performed with slight modifications of a

protocol described previously (29). Briefly, parasites were grown in the absence or presence of ATc for 3-4 days, mechanically egressed from host cells through a 26 gauge needle, filtered through a 3 µm polycarbonate filter to remove host cell debris, washed once in base medium (Agilent Technologies) supplemented with 1 mM L-glutamine and 5 mM D-glucose, then resuspended in base medium to 1.5×10^7 cells/ml. 1.5×10^6 parasites were seeded into wells of a Seahorse XFe96 cell culture plates coated with 3.5 µg/cm^2 CellTak cell adhesive (Corning), and attached to the bottom of wells by centrifugation at 800 × *g* for 3 min. Final volumes in wells were made up to 175 µl with supplemented base medium. ETC inhibitors were loaded into the sensor cartridge ports, and injected into wells at designated points during the experiment. OCR and ECAR measurements were obtained every 3 min for 5 repeats before and after injection of compounds. Injections 1 and 2 contained 1 µM carbonyl cyanide-p-trifluoromethoxyphenylhydrazone (FCCP; Sigma) and 1 µM atovaquone (Sigma), respectively. The basal mOCR was calculated by subtracting the non-mitochondrial OCR (the value following atovaquone addition) from the basal OCR value obtained. A minimum of 4 background wells were used in each plate, and 3 technical replicates (i.e. wells subjected to identical treatments) were used for each condition.

Statistical and data analyses

Statistical differences between conditions differing in the presence or absence of ATc (free heme and cellular ATP levels) were tested through application of unpaired two-tailed Student's *t*-tests as described in the relevant sections.

Data from the Seahorse flux analysis were compiled and exported from the Seahorse Wave Desktop software (Agilent Technologies). A linear mixed effects model was applied to the data (29), setting the error between plates (between experiments) and wells (within experiments) as random effects, and the mOCR or ECAR values between cell lines and days on drug (ATc) as fixed effects. Analysis of the least square means of the values were performed on the R software environment. Statistical differences in these values were tested through ANOVA (linear mixed effects), with a post hoc Tukey test.

ACKNOWLEDGEMENTS

We thank Gary Ward for providing the anti-GRA8 antibody, and Harpreet Vohra and Michael Devoy for performing fluorescence activated cell sorting.

CONFLICTS OF INTEREST

We hereby declare no conflicts of interests within this article.

REFERENCES

1. McFadden, G. I., and Roos, D. S. (1999) Apicomplexan plastids as drug targets. *Trends Microbiol* **7**, 328-333
2. Ralph, S. A., van Dooren, G. G., Waller, R. F., Crawford, M. J., Fraunholz, M. J., Foth, B. J., Tonkin, C. J., Roos, D. S., and McFadden, G. I. (2004) Tropical infectious diseases: Metabolic maps and functions of the *Plasmodium falciparum* apicoplast. *Nat Rev Microbiol* **2**, 203-216
3. Sato, S. (2011) The apicomplexan plastid and its evolution. *Cell Mol Life Sci* **68**, 1285-1296
4. Janouskovec, J., Horak, A., Obornik, M., Lukes, J., and Keeling, P. J. (2010) A common red algal origin of the apicomplexan, dinoflagellate, and heterokont plastids. *Proc Natl Acad Sci U S A* **107**, 10949-10954

5. van Dooren, G. G., and Striepen, B. (2013) The algal past and parasite present of the apicoplast. *Annu Rev Microbiol* **67**, 271-289
6. Janouskovec, J., Paskerova, G. G., Miroliubova, T. S., Mikhailov, K. V., Birley, T., Aleoshin, V. V., and Simdyanov, T. G. (2019) Apicomplexan-like parasites are polyphyletic and widely but selectively dependent on cryptic plastid organelles. *Elife* **8**, e49662
7. Sigala, P. A., and Goldberg, D. E. (2014) The peculiarities and paradoxes of *Plasmodium* heme metabolism. *Annu Rev Microbiol* **68**, 259-278
8. van Dooren, G. G., Kennedy, A. T., and McFadden, G. I. (2012) The use and abuse of heme in apicomplexan parasites. *Antioxid Redox Signal* **17**, 634-656
9. Koreny, L., Obornik, M., and Lukes, J. (2013) Make it, take it, or leave it: heme metabolism of parasites. *PLoS Pathog* **9**, e1003088
10. Hayward, J. A., and van Dooren, G. G. (2019) Same same, but different: Uncovering unique features of the mitochondrial respiratory chain of apicomplexans. *Mol Biochem Parasitol* **232**, 111204
11. Seeber, F., Limenitakis, J., and Soldati-Favre, D. (2008) Apicomplexan mitochondrial metabolism: a story of gains, losses and retentions. *Trends Parasitol* **24**, 468-478
12. Koreny, L., Sobotka, R., Janouskovec, J., Keeling, P. J., and Obornik, M. (2011) Tetrapyrrole synthesis of photosynthetic chromerids is likely homologous to the unusual pathway of apicomplexan parasites. *Plant Cell* **23**, 3454-3462
13. Varadharajan, S., Dhanasekaran, S., Bonday, Z. Q., Rangarajan, P. N., and Padmanaban, G. (2002) Involvement of delta-aminolaevulinate synthase encoded by the parasite gene in de novo haem synthesis by *Plasmodium falciparum*. *Biochem J* **367**, 321-327
14. Ke, H., Sigala, P. A., Miura, K., Morrisey, J. M., Mather, M. W., Crowley, J. R., Henderson, J. P., Goldberg, D. E., Long, C. A., and Vaidya, A. B. (2014) The heme biosynthesis pathway is essential for *Plasmodium falciparum* development in mosquito stage but not in blood stages. *J Biol Chem* **289**, 34827-34837
15. Nagaraj, V. A., Prasad, D., Rangarajan, P. N., and Padmanaban, G. (2009) Mitochondrial localization of functional ferrochelatase from *Plasmodium falciparum*. *Mol Biochem Parasitol* **168**, 109-112
16. Nagaraj, V. A., Sundaram, B., Varadarajan, N. M., Subramani, P. A., Kalappa, D. M., Ghosh, S. K., and Padmanaban, G. (2013) Malaria parasite-synthesized heme is essential in the mosquito and liver stages and complements host heme in the blood stages of infection. *PLoS Pathog* **9**, e1003522
17. Rathnapala, U. L., Goodman, C. D., and McFadden, G. I. (2017) A novel genetic technique in *Plasmodium berghei* allows liver stage analysis of genes required for mosquito stage development and demonstrates that *de novo* heme synthesis is essential for liver stage development in the malaria parasite. *PLoS Pathog* **13**, e1006396
18. Rizopoulos, Z., Matuschewski, K., and Haussig, J. M. (2016) Distinct Prominent Roles for Enzymes of *Plasmodium berghei* Heme Biosynthesis in Sporozoite and Liver Stage Maturation. *Infect Immun* **84**, 3252-3262
19. Shanmugam, D., Wu, B., Ramirez, U., Jaffe, E. K., and Roos, D. S. (2010) Plastid-associated porphobilinogen synthase from *Toxoplasma gondii*: kinetic and structural properties validate therapeutic potential. *J Biol Chem* **285**, 22122-22131
20. van Dooren, G. G., Su, V., D'Ombrain, M. C., and McFadden, G. I. (2002) Processing of an apicoplast leader sequence in *Plasmodium falciparum* and the identification of a putative leader cleavage enzyme. *J Biol Chem* **277**, 23612-23619
21. van Dooren, G. G., Tomova, C., Agrawal, S., Humbel, B. M., and Striepen, B. (2008) *Toxoplasma gondii* Tic20 is essential for apicoplast protein import. *Proc Natl Acad Sci U S A* **105**, 13574-13579
22. Masuda, T., and Takahashi, S. (2006) Chemiluminescent-based method for heme determination by reconstitution with horseradish peroxidase apo-enzyme. *Anal Biochem* **355**, 307-309

23. Dumont, M. E., Cardillo, T. S., Hayes, M. K., and Sherman, F. (1991) Role of cytochrome c heme lyase in mitochondrial import and accumulation of cytochrome c in *Saccharomyces cerevisiae*. *Mol Cell Biol* **11**, 5487-5496
24. van Dooren, G. G., Yeoh, L. M., Striepen, B., and McFadden, G. I. (2016) The Import of Proteins into the Mitochondrion of *Toxoplasma gondii*. *J Biol Chem* **291**, 19335-19350
25. Sidik, S. M., Huet, D., Ganesan, S. M., Huynh, M. H., Wang, T., Nasamu, A. S., Thiru, P., Saeij, J. P., Carruthers, V. B., Niles, J. C., and Lourido, S. (2016) A genome-wide CRISPR screen in *Toxoplasma* identifies essential apicomplexan genes. *Cell* **166**, 1423-1435
26. Huet, D., Rajendran, E., van Dooren, G. G., and Lourido, S. (2018) Identification of cryptic subunits from an apicomplexan ATP synthase. *eLife* **7**, e38097
27. Brooks, C. F., Johnsen, H., van Dooren, G. G., Muthalagi, M., Lin, S. S., Bohne, W., Fischer, K., and Striepen, B. (2010) The *Toxoplasma* apicoplast phosphate translocator links cytosolic and apicoplast metabolism and is essential for parasite survival. *Cell Host Microbe* **7**, 62-73
28. Pasini, E. M., van den Ierssel, D., Vial, H. J., and Kocken, C. H. (2013) A novel live-dead staining methodology to study malaria parasite viability. *Malar J* **12**, 190
29. Seidi, A., Muellner-Wong, L. S., Rajendran, E., Tjhin, E. T., Dagley, L. F., Aw, V. Y., Faou, P., Webb, A. I., Tonkin, C. J., and van Dooren, G. G. (2018) Elucidating the mitochondrial proteome of *Toxoplasma gondii* reveals the presence of a divergent cytochrome c oxidase. *eLife* **7**, e38131
30. Zhang, J., Nuebel, E., Wisidagama, D. R., Setoguchi, K., Hong, J. S., Van Horn, C. M., Imam, S. S., Vergnes, L., Malone, C. S., Koehler, C. M., and Teitell, M. A. (2012) Measuring energy metabolism in cultured cells, including human pluripotent stem cells and differentiated cells. *Nat Protoc* **7**, 1068-1085
31. Bergmann, A., Floyd, K., Key, M., Dameron, C., C., R. K., Whitehead, D. C., Hamza, I., and Dou, Z. (2019) *Toxoplasma gondii* requires its plant-like heme biosynthesis pathway for infection. *BioRxiv*, 10.1101/753863
32. van Dooren, G. G., and Hapuarachchi, S. V. (2017) The dark side of the chloroplast: biogenesis, metabolism and membrane biology of the apicoplast. in *Advances in Botanical Research* (Hirakawa, Y. ed.), Academic Press, Oxford. pp 145-185
33. Beckers, C. J., Roos, D. S., Donald, R. G., Luft, B. J., Schwab, J. C., Cao, Y., and Joiner, K. A. (1995) Inhibition of cytoplasmic and organellar protein synthesis in *Toxoplasma gondii*. Implications for the target of macrolide antibiotics. *J Clin Invest* **95**, 367-376
34. Badminton, M. N., and Elder, G. H. (2009) Inherited disorders of haem synthesis: the human porphyrias. in *Tetrapyrroles: Birth, Life and Death* (Warren, M. J., and Smith, A. G. eds.), Landes Bioscience, Austin. pp 89-100
35. Kauppinen, R. (2005) Porphyrias. *Lancet* **365**, 241-252
36. Singal, A. K. (2019) Porphyria cutanea tarda: Recent update. *Mol Genet Metab* **128**, 271-281
37. Sigala, P. A., Crowley, J. R., Henderson, J. P., and Goldberg, D. E. (2015) Deconvoluting heme biosynthesis to target blood-stage malaria parasites. *Elife* **4**, e09143
38. Jacot, D., Waller, R. F., Soldati-Favre, D., MacPherson, D. A., and MacRae, J. I. (2015) Apicomplexan Energy Metabolism: Carbon Source Promiscuity and the Quiescence Hyperbole. *Trends Parasitol* **32**, 56-70
39. Lin, S. S., Blume, M., von Ahsen, N., Gross, U., and Bohne, W. (2011) Extracellular *Toxoplasma gondii* tachyzoites do not require carbon source uptake for ATP maintenance, gliding motility and invasion in the first hour of their extracellular life. *Int J Parasitol* **41**, 835-841
40. MacRae, J. I., Sheiner, L., Nahid, A., Tonkin, C., Striepen, B., and McConville, M. J. (2012) Mitochondrial metabolism of glucose and glutamine is required for intracellular growth of *Toxoplasma gondii*. *Cell Host Microbe* **12**, 682-692
41. Nitzsche, R., Zagoriy, V., Lucius, R., and Gupta, N. (2016) Metabolic cooperation of glucose and glutamine is essential for the lytic cycle of obligate intracellular parasite *Toxoplasma gondii*. *J Biol Chem* **291**, 126-141

42. Shukla, A., Olszewski, K. L., Llinas, M., Rommereim, L. M., Fox, B. A., Bzik, D. J., Xia, D., Wastling, J., Beiting, D., Roos, D. S., and Shanmugam, D. (2018) Glycolysis is important for optimal asexual growth and formation of mature tissue cysts by *Toxoplasma gondii*. *Int J Parasitol* **48**, 955-968
43. Uboldi, A. D., McCoy, J. M., Blume, M., Gerlic, M., Ferguson, D. J., Dagley, L. F., Beahan, C. T., Stapleton, D. I., Gooley, P. R., Bacic, A., Masters, S. L., Webb, A. I., McConville, M. J., and Tonkin, C. J. (2015) Regulation of Starch Stores by a Ca(2+)-Dependent Protein Kinase Is Essential for Viable Cyst Development in *Toxoplasma gondii*. *Cell Host Microbe* **18**, 670-681
44. Steiner, H., Kispal, G., Zollner, A., Haid, A., Neupert, W., and Lill, R. (1996) Heme binding to a conserved Cys-Pro-Val motif is crucial for the catalytic function of mitochondrial heme lyases. *J Biol Chem* **271**, 32605-32611
45. Kranz, R., Lill, R., Goldman, B., Bonnard, G., and Merchant, S. (1998) Molecular mechanisms of cytochrome c biogenesis: three distinct systems. *Mol Microbiol* **29**, 383-396
46. Harding, C. R., Sidik, S. M., Petrova, B., Gnadig, N. F., Okombo, J., Ward, K. E., Markus, B. M., Fidock, D. A., and Lourido, S. (2019) Genetic screens reveal a central role for heme biosynthesis in artemisinin susceptibility. *bioRxiv*, 10.1101/746974
47. Jacot, D., Meissner, M., Sheiner, L., Soldati-Favre, D., and Striepen, B. (2014) Genetic manipulation of *Toxoplasma gondii*. in *Toxoplasma gondii: the model apicomplexan* (Weiss, L. M., and Kim, K. eds.), Elsevier, Amsterdam. pp 577-611
48. Gubbels, M. J., Li, C., and Striepen, B. (2003) High-throughput growth assay for *Toxoplasma gondii* using yellow fluorescent protein. *Antimicrob Agents Chemother* **47**, 309-316
49. Rajendran, E., Hapuarachchi, S. V., Miller, C. M., Fairweather, S. J., Cai, Y., Smith, N. C., Cockburn, I. A., Broer, S., Kirk, K., and van Dooren, G. G. (2017) Cationic amino acid transporters play key roles in the survival and transmission of apicomplexan parasites. *Nat Commun* **8**, 14455
50. Sheiner, L., Demerly, J. L., Poulsen, N., Beatty, W. L., Lucas, O., Behnke, M. S., White, M. W., and Striepen, B. (2011) A systematic screen to discover and analyze apicoplast proteins identifies a conserved and essential protein import factor. *PLoS Pathog* **7**, e1002392
51. Huynh, M. H., and Carruthers, V. B. (2009) Tagging of endogenous genes in a *Toxoplasma gondii* strain lacking Ku80. *Eukaryot Cell* **8**, 530-539
52. Katris, N. J., van Dooren, G. G., McMillan, P. J., Hanssen, E., Tilley, L., and Waller, R. F. (2014) The apical complex provides a regulated gateway for secretion of invasion factors in *Toxoplasma*. *PLoS Pathog* **10**, e1004074
53. Carey, K. L., Donahue, C. G., and Ward, G. E. (2000) Identification and molecular characterization of GRA8, a novel, proline-rich, dense granule protein of *Toxoplasma gondii*. *Mol Biochem Parasitol* **105**, 25-37
54. Agrawal, S., van Dooren, G. G., Beatty, W. L., and Striepen, B. (2009) Genetic evidence that an endosymbiont-derived endoplasmic reticulum-associated protein degradation (ERAD) system functions in import of apicoplast proteins. *J Biol Chem* **284**, 33683-33691
55. Fruk, L., Kuhlmann, J., and Niemeyer, C. M. (2009) Analysis of heme-reconstitution of apoenzymes by means of surface plasmon resonance. *Chem Commun (Camb)*, 230-232
56. Teale, F. W. (1959) Cleavage of the haem-protein link by acid methylethylketone. *Biochim Biophys Acta* **35**, 543

Footnotes

[2] The abbreviations used are: ALA, δ-aminolevulinic acid; ATc, anhydrotetracycline; ANOVA, analysis of variance; CCCP, carbonyl cyanide 3-chlorophenylhydrazone; CCHL, cytochrome *c*/*c*$_1$ heme lyase; Cyt c, cytochrome *c*; Cyt *c*$_1$, cytochrome c$_1$; $\Delta\Psi_m$, mitochondrial membrane potential; DMEM, Dulbecco's modified Eagle's medium; ECAR, extracellular acidification rate; ETC, electron transport chain; FCCP, carbonyl cyanide-p-trifluoromethoxyphenylhydrazone; HFF, human foreskin fibroblasts; HRP, horseradish peroxidase; JC-1, 5,5',6,6'-Tetrachloro-1,1',3,3'-tetraethylbenzimidazolyl-carbocyanine iodide; mOCR, mitochondrial O_2 consumption rate; UroD, uroporphyrinogen III decarboxylase.

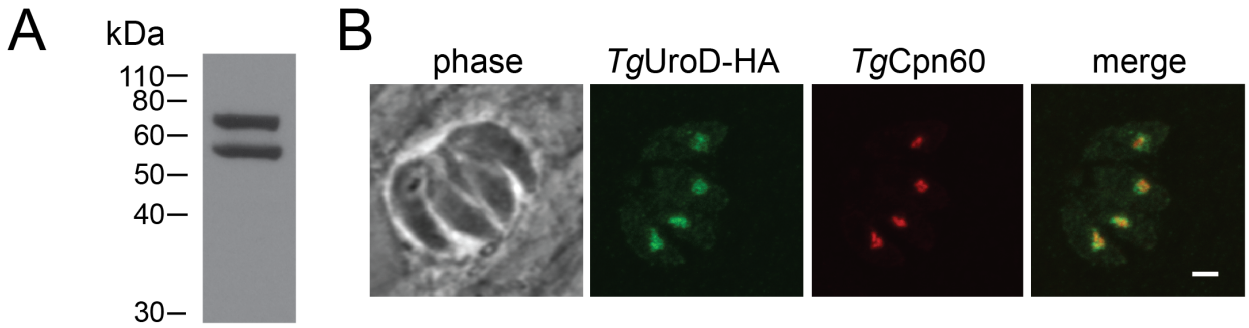

Figure 1. Expression and localization of *Tg*UroD in *T. gondii*. (A) Western blot of proteins extracted from *Tg*UroD-HA parasites in *T. gondii* tachyzoites and probed with anti-HA antibodies. **(B)** Immunofluorescence assay of four intracellular *T. gondii* parasites located within the same parasitophorous vacuole. *Tg*UroD-HA (green) co-localizes with an apicoplast marker *Tg*Cpn60 (red). Scale bar is 2 µm.

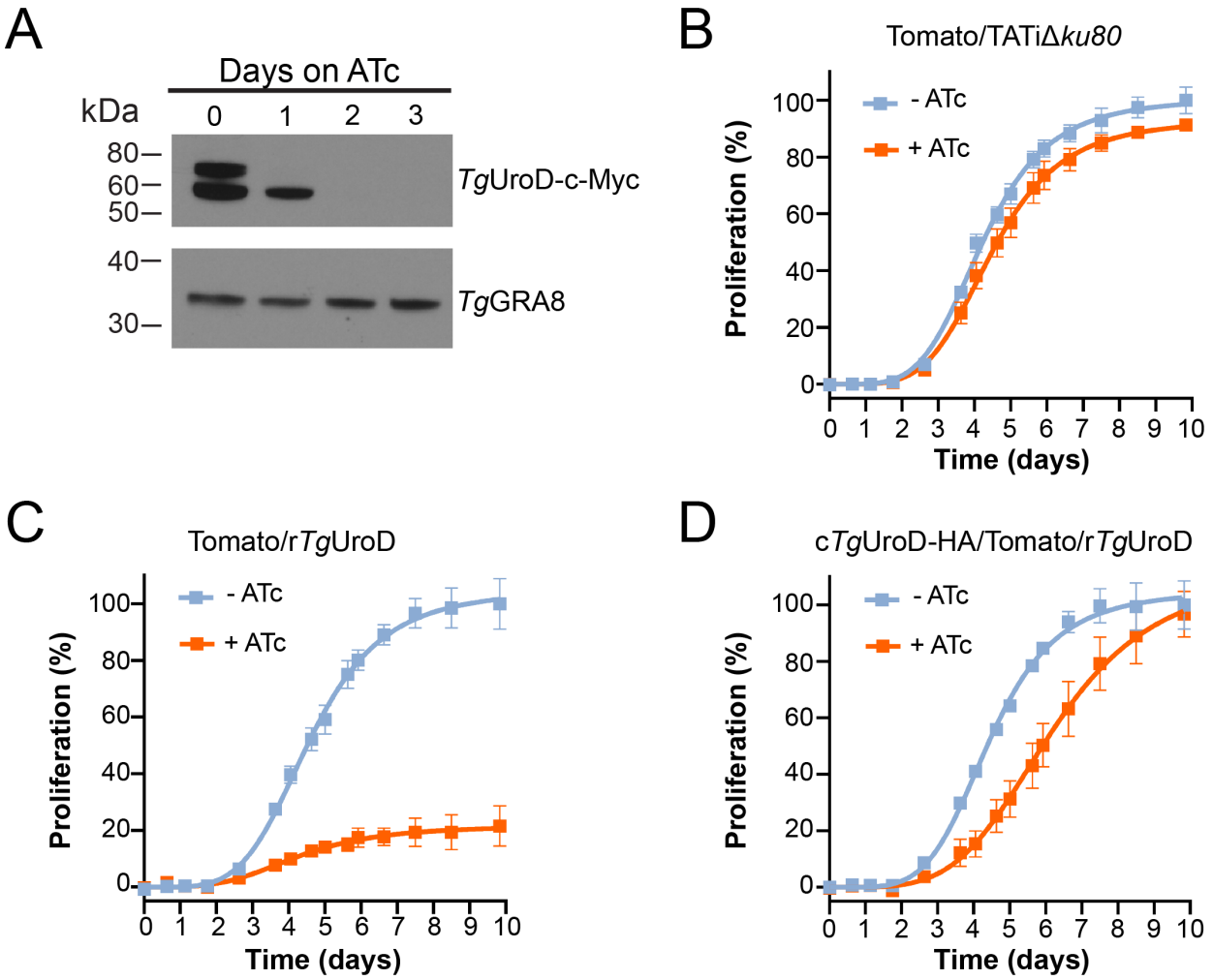

Figure 2. Knockdown of *Tg*UroD causes a defect in parasite proliferation. (A) Western blot of the r*Tg*UroD-c-Myc line grown in the presence of ATc for 0-3 days and probed with antibodies again c-Myc (to detect r*Tg*UroD-c-Myc) and *Tg*GRA8 (as a loading control). **(B-D)** Fluorescence growth assays depicting parasite proliferation in **(B)** parental Tomato/TATiΔ*ku80*, **(C)** Tomato/r*Tg*UroD, and **(D)** c*Tg*UroD-HA/Tomato/r*Tg*UroD strain parasites grown in the absence (blue) or presence (orange) of ATc. Proliferation is expressed as a percentage of that measured in parasites grown in the absence of ATc on the final day of each experiment. Data depict the mean ± SD from three technical replicates and are representative of three independent experiments.

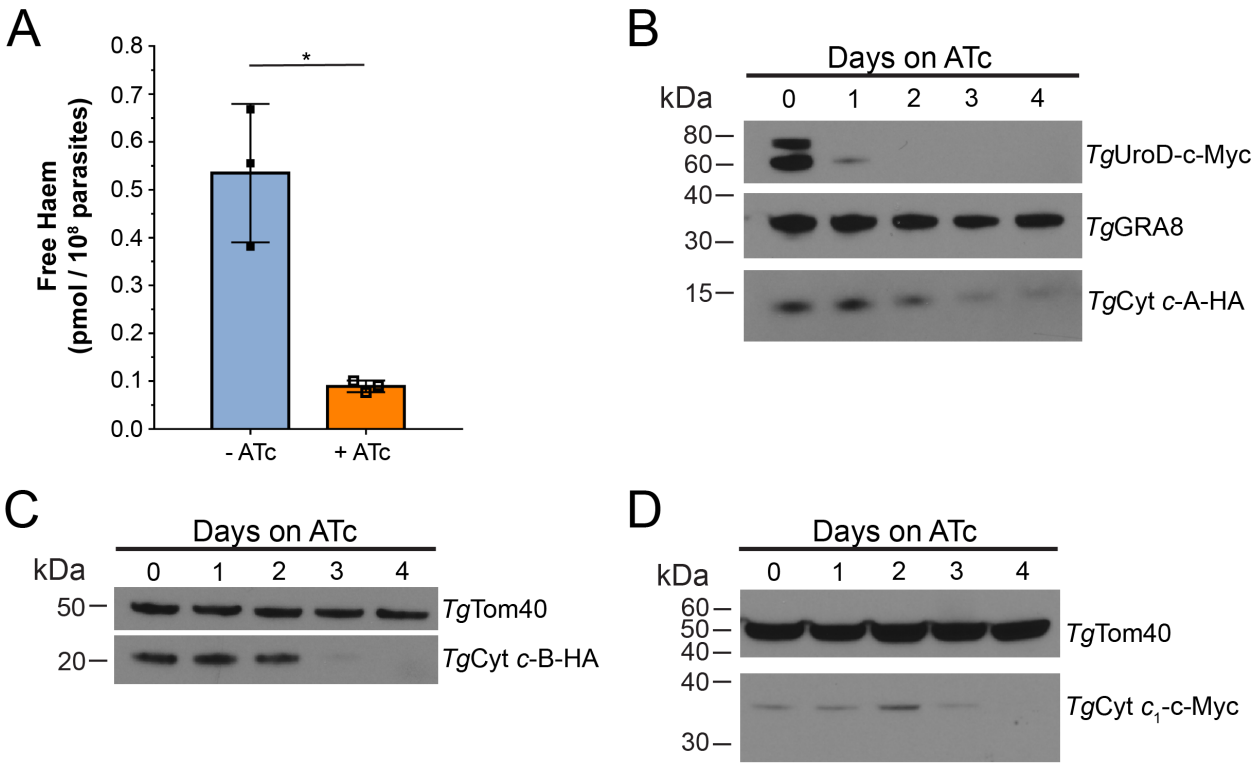

Figure 3. Knockdown of *Tg*UroD reduces free heme and mitochondrial *c*-type cytochrome abundance in parasites. (A) Free heme levels were measured in parasites grown in the absence (blue) or presence (orange) of ATc for 3 days. Data show the mean ± SD from three independent experiments (* $P < 0.05$; two-tailed unpaired Student's *t*-test). **(B)** Western blots of r*Tg*UroD-c-myc/*Tg*Cyt *c*-A-HA parasites grown in the presence of ATc for 0-4 days and probed with antibodies against c-Myc, HA and *Tg*GRA8 (loading control). **(C)** Western blots of r*Tg*UroD/*Tg*Cyt *c*-B-HA parasites grown in the presence of ATc for 0-4 days and probed with antibodies against HA and anti-*Tg*Tom40 (loading control). **(D)** Western blots of r*Tg*UroD/*Tg*Cyt c_1-c-Myc parasites grown in the presence of ATc for 0-4 days and probed with antibodies against c-Myc and anti-*Tg*Tom40 (loading control). All western blots are representative of three independent experiments.

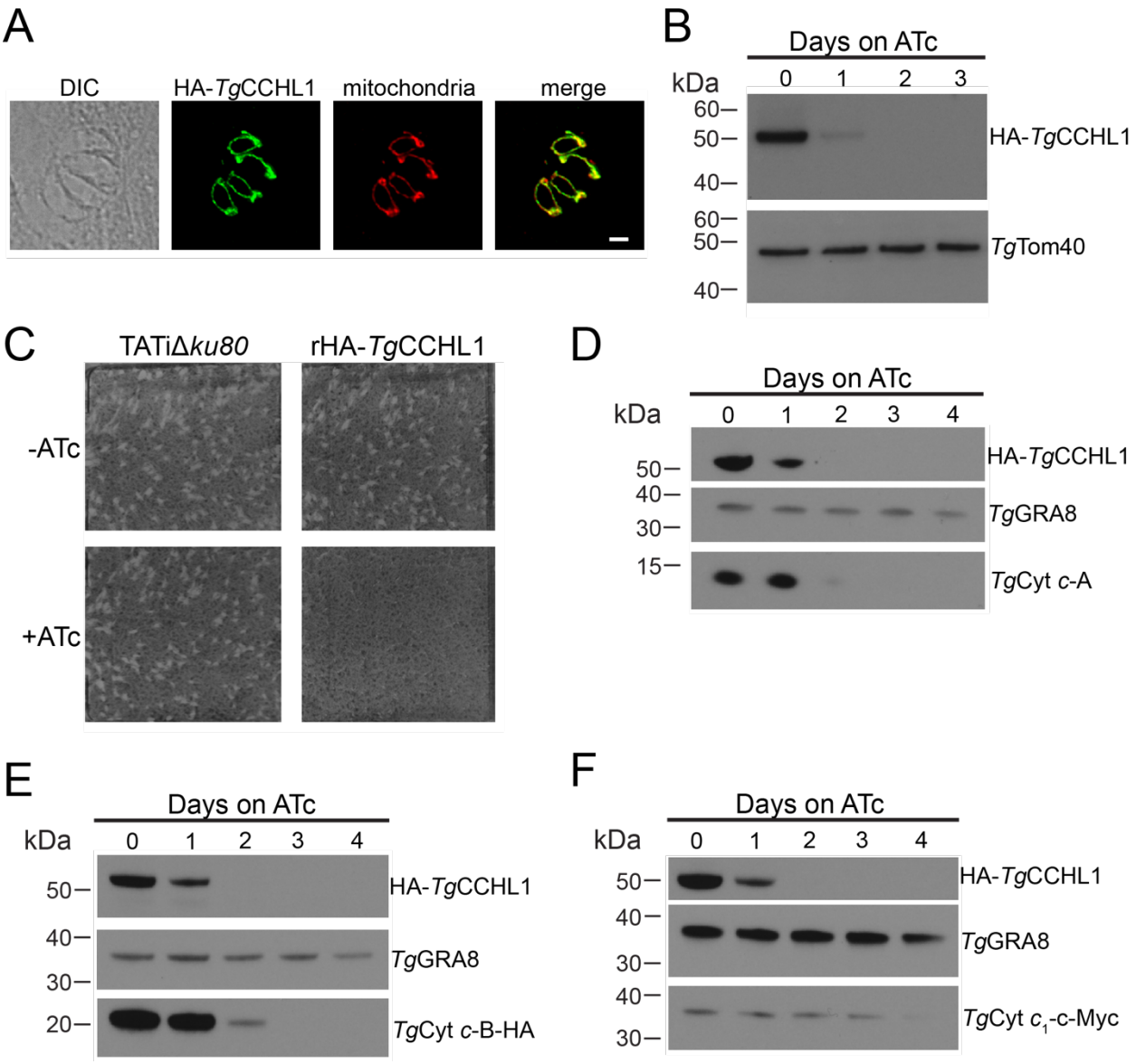

Figure 4. Knockdown of *Tg*CCHL1 results in defects in parasite proliferation and a depletion in the abundance of *c*-type cytochromes (A) Immunofluorescence assay of a four cell parasite vacuole with HA-*Tg*CCHL1 (green) co-localizing with the mitochondrial marker Tom40 (red). Scale bar is 2 µm. **(B)** Western blots of iHA$_3$-*Tg*CCHL1 lines grown in the presence of ATc for 0-3 days and probed with antibodies against HA and *Tg*Tom40 (as a loading control). (**C)** Plaque assay of parental TATiΔ*ku80* and rHA-*Tg*CCH1L parasites grown in the absence or presence of ATc over 8 days. Data are from a single experiment and representative of three independent experiments. **(D-F)** Western blots of rHA$_3$-*Tg*CCHL1 parasite strains grown in the presence of ATc for 0-4 days and probed with antibodies against **(D)** *Tg*Cyt *c*-A, **(E)** HA-tagged *Tg*Cyt *c*-B, and **(F)** c-Myc-tagged *Tg*Cyt c_1. GRA8 is included as a loading control, and data are representative of three independent experiments.

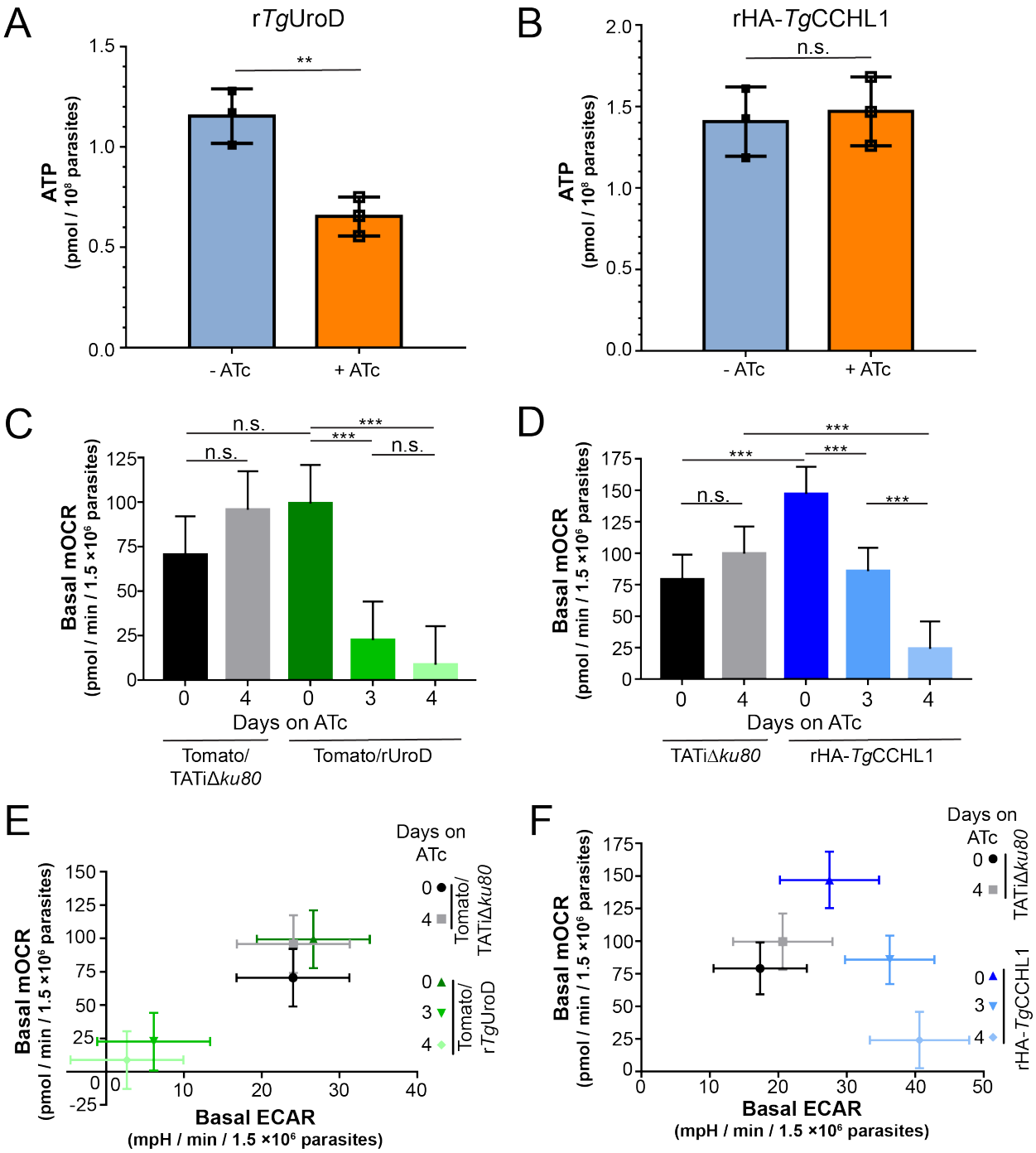

Figure 5. Knockdown of *Tg*UroD leads to general metabolic defects in parasites, whereas knockdown of *Tg*CCHL1 results in selective defects in the mitochondrial ETC. (A-B) Whole cell ATP levels were measured in r*Tg*UrOD **(A)** and rHA-*Tg*CCHL1 **(B)** parasites grown in the absence of ATc (blue) or the presence of ATc for 3 days (orange). Data show the mean ± SD from three independent experiments (** $P < 0.01$; n.s. = not significant $P > 0.05$; two-tailed unpaired Student's *t*-test). **(C-D)** Basal mitochondrial oxygen consumption rates (mOCR) in **(C)** Tomato/TATiΔ*ku80* parental (black/gray) and r*Tg*UroD (green) parasites, or **(D)** TATiΔ*ku80* parental (black/gray) and rHA-*Tg*CCHL1 parasites (blue) grown in the absence of ATc or the presence of ATc for 3 or 4 days. Data depict the least square

means from a linear mixed model ± 95% confidence limits from 3 independent experiments (*** $P < 0.001$; n.s. = not significant, $P > 0.05$; ANOVA with Tukey's post hoc test). **(E-F)** Basal mOCR plotted against basal ECAR in **(E)** Tomato/TATiΔ*ku80* parental (black/gray) and r*Tg*UroD (green) parasites, or **(F)** TATiΔ*ku80* parental (black/gray) and rHA-*Tg*CCHL1 parasites (blue). Parasites were grown in the absence of ATc, or in the presence of ATc for 3 or 4 days. Data depict the least square means from a linear mixed model ± 95% confidence limits from 3 independent experiments.